Energy Conversion and Management 251 (2022) 114914

Contents lists available at ScienceDirect

Energy Conversion and Management

journal homepage: www.elsevier.com/locate/enconman

Optimal strategies of deployment of far offshore co-located wind-wave energy farms

Aitor Saenz-Aguirre [a,*], Jon Saenz [b,d], Alain Ulazia [a], Gabriel Ibarra-Berastegui [c,d]

[a] Energy Engineering Department, University of the Basque Country (UPV/EHU). Otaola Hiribidea 29, 20600 Eibar, Spain
[b] Department of Physhics, University of the Basque Country (UPV/EHU). Sarriena, 48940 Leioa, Spain
[c] Energy Engineering Department, University of the Basque Country (UPV/EHU). Alda. Urkijo, 48013 Bilbao, Spain
[d] Plentziako Itsas Estazioa (BEGIK), University of Basque Country (UPV/EHU). Areatza Hiribidea 47, 48620 Plentzia, Spain

ARTICLE INFO

Keywords:
Far offshore
Hydrogen production
Wave energy
Wind energy
Point absorber
ERA5
Maximum covariance analysis
Fluid mechanics

ABSTRACT

The most profitable offshore energy resources are usually found away from the coast. Nevertheless, the accessibility and grid integration in those areas are more complicated. To avoid this problematic, large scale hydrogen production is being promoted for far offshore applications. The main objective of this paper is to analyze the ability of wave energy converters to maximize hydrogen production in hybrid wind and wave far offshore farms. To that end, wind and wave resource data are obtained from *ERA5* for different locations in the Atlantic ocean and a Maximum Covariance Analysis is proposed for the selection of the most representative locations. Furthermore, the suitability of different sized wave energy converters for auxiliary hydrogen production in the far offshore wind farms is also analysed. On that account, the hydrodynamic parameters of the oscillating bodies are obtained via simulations with a Boundary Element Method based code and their operation is modelled using the software tool Matlab. The combination of both methodologies enables to perform a realistic assessment of the contribution of the wave energy converters to the hydrogen generation of an hybrid energy farm, especially during those periods when the wind turbines would be stopped due to the variability of the wind. The obtained results show a considerable hydrogen generation capacity of the wave energy converters, up to 6.28% of the wind based generation, which could remarkably improve the efficiency of the far offshore farm and bring important economical profit. Wave energy converters are observed to be most profitable in those farms with low covariance between wind and waves, where the disconnection times of the wind turbines are prone to be more prolonged but the wave energy is still usable. In such cases, a maximum of 101.12 h of equivalent rated production of the wind turbine has been calculated to be recovered by the wave energy converters.

1. Introduction

Offshore renewable energy is expected to play an important role in the transition towards strict sustainability of the electrical energy generation in the near future. Nowadays, wind is the most profitable and industrially mature offshore renewable energy source [1]. The offshore wind technology has undergone a remarkable development during the last years, with wind farms scaled up to 1000 MW [2]. On the one hand, in comparison to onshore technology, offshore wind turbines usually receive higher and less turbulent wind speeds and have no restrictions due to mechanical noise. Hence, they usually achieve a higher Annual Energy Production (AEP). On the other hand, the economical investment necessary for the installation of offshore wind turbines is higher, and difficulties related to their assembly and accessibility arise as well, due to their location in the sea.

In addition to offshore wind turbines, ocean energy (wave and tidal energy) is also presented in the literature as a growing and developing technology [3]. Under the assumption of an energy conversion efficiency of 40% and a wave power density above 30 kW/m in the 2% of the world's coasts, the power which can be achieved by ocean energy is estimated to be larger than 500 GW [4]. If the rest of the coastal line and the far offshore plants were additionally considered, the power production associated to ocean energy would significantly increase. In fact, the ocean energy sector plans to promote green energy generation projects of up to 100 GW for the year 2050 [1].

Regarding wave energy, Wave Energy Converters (WECs) are used to convert the kinetic or potential energy of the water into electrical

* Corresponding author.
E-mail addresses: aitor.saenz@ehu.eus (A. Saenz-Aguirre), jon.saenz@ehu.eus (J. Saenz), alain.ulazia@ehu.eus (A. Ulazia), gabriel.ibarra@ehu.eus (G. Ibarra-Berastegui).

https://doi.org/10.1016/j.enconman.2021.114914
Received 21 May 2021; Received in revised form 9 October 2021; Accepted 19 October 2021
Available online 12 November 2021

Nomenclature

f_{PTO}	Force induced by the PTO system
f_{PTOmax}	Maximum force the PTO system can generate
$\left\|\overrightarrow{F}\right\|$	Wave Energy Flux
H_s	Significant wave height
M	Total mass of the floating buoy and the reaction plate
P	Power generated by the WEC
R^2	Fraction of variance
T_p	Peak wave period
$\overline{T}$	Mean wave period
U	Wind speed
W	Wind power density
z	In heave displacement of the point absorber
z_{max}	Maximum in heave displacement of the point absorber
η	In heave elevation of the wave
λ	Longitude
φ	Latitude
ρ	Air density

Abbreviations

ACF	AutoCorrelation Function
AEP	Annual Energy Production
AO	Artic Oscillation
BEM	Boundary Element Method
CDS	Climate Data Store
HAWT	Horizontal Axis Wind Turbine
LCOE	Levelised Cost of Energy
MCA	Maximum Covariance Analysis
MHK	Marine HydroKinetic
MPC	Model Predictive Control
NAO	North Atlantic Oscillation
NREL	National Renewable Energies Laboratory
OWC	Oscillating Water Column
PS	PseudoSpectral
PTO	Power Take-Off
RM3	Reference Model 3
SGD	Sustainable Development Goal
WEC	Wave Energy Converter
WEF	Wave Energy Flux
WPD	Wind Power Density

energy. A detailed review of the existing WEC technologies is presented by Falcao [5]. These technologies can be divided in three main groups: Overtopping converters (the wave oscillations are used to store water in a reservoir above water level and then convert it into electrical energy), Oscillating Water Columns (OWCs) (wave oscillations produce an air flow in a chamber that, in turn, causes rotation of a turbine) and point absorbers (oscillating bodies which swing with the waves and transform their mechanical motion into electrical energy).

The design and performance of point absorbers with different geometries have been widely studied in the literature: One body linear point absorber [6], gyroscope-based inertial point absorbers [7], vertical axis pendulum based WEC [8] or a two-body linear point absorber [9] constitute nice examples of this kind of studies. The operation of point absorbers is regulated by means of a Power Take-Off (PTO) system, which controls the motion of the oscillating body and ensures the quality of the generated energy. Since the potential response of the PTO system is generally subject to constraints of different nature, it is important to consider the PTO when examining the operation and power generation of the WEC. Several PTO control strategies applied to WECs have been described in the literature, such as Model Predictive Control (MPC) [10], nonlinear control [11], robust control [12] or improved latching control [13] to mention a few.

The main drawbacks linked to offshore energy generation systems are the complicated accessibility, material transportation and the need of mooring/anchoring. Despite of them, the development and installation of multi-megawatt bottom-fixed [14] and floating offshore wind turbines [15] is already a reality. In case of installation of far offshore generators (>90 km from the coast), the main challenge is the energy storage, due to the difficulties associated to the grid integration. In this way, techno-economic feasibility studies that endorse the installation of such far offshore energy generation farms can be found in the literature [16]. The use of different energy storage methods is analysed in detail in the aforementioned study. The installation of far offshore wind turbines has also been addressed in wind energy related international industrial congresses [17]. To avoid the difficulties associated to the anchoring/mooring in far offshore locations, mobile offshore energy harvesting solutions have been proposed as well. These mobile technologies can be divided in two main groups: Sailing wind turbines [16] (the power is produced by a wind turbine located in the ship) and energy ships [18] (the power is produced by a turbine located at the hull of a wind propelled ship).

The installation of integrated offshore wind turbine and WEC systems, considering their cross-couplings, has also been proposed in the literature. In fact, this topic is gaining much prominence among future developments of the offshore energy [19]. A detailed review of the economical feasibility of the wave energy is presented by Astariz et al. [20]. This review concludes that the installation of combined wind and wave energy systems is the best way to increase the efficiency of marine resource exploitation systems and increase their competitiveness. Ireland is already a well-known location due to its potential for co-located wind and wave farms. The low correlation between wind/wave resources in Northwest and Southwest of this island can be successfully exploited, since co-located energy farms offer a more predictable, less variable renewable energy source [21]. This promising low variability of energy due to combination of wind and waves have been also detected in other island environments [22], continental nearshore areas in China or Denmark [23], and even in closed seas such as the Mediterranean or the Caspian sea [24]. In order to extend these studies, this paper takes these type of studies to the next level, analyzing the combination of wind and wave energies in far offshore locations in the Atlantic ocean.

The energy storage in far offshore locations, as shown by Babarit et al. [16], can be successfully and competitively accomplished using various energy vectors. Moreover, the use of energy vectors in standalone energy generation systems is known to help alleviate the intermittent nature of the offshore resource itself, which subsequently implies intermittent electricity generation patterns [25]. Many studies have highlighted the huge potential of hydrogen for the management and regulation of offshore [26] and far offshore [16] renewable energy generation systems. Due to its consideration as the fuel of the future, hydrogen [27] is being promoted by many governments and international companies. A recent study for France [28] suggests that a spatial planning at a regional level of different renewable sources might be needed to maximize the hydrogen production by 2035. The European Union published in 2020 a hydrogen promotion strategy by which the objective is to install in Europe 40 GW of renewable energy hydrogen electrolysers and an storage of up to 10 million tons of this fuel for years 2025–2030 [29]. In this context, many examples of hydrogen generation applied to offshore wind and wave energy farms have been found in the literature [30]. The main elements involved in the hydrogen generation process [30] are the power generator, sea water electrolyser, fuel cell and energy accumulator. In the case of far offshore applications,

hydrogen production applied to wind turbines placed on sailing ships have also been analysed in the literature [31]. Drawbacks of hydrogen generation, and its subsequent use as a power source [32], lie especially in terms of storage and transportation safety. In response to that, recent developments also suggest that other energy vectors, such as methanol [33], could overcome some of these difficulties and improve the functionality of the hydrogen as a fuel [34].

The main objective of this paper is to make a quantitative assessment of the real performance and energy generation of different sized WECs (using a generic PTO) as auxiliary hydrogen producers in an hybrid wind-wave energy farm. The power produced by a WEC is usually significantly lower than the one produced by a wind turbine. Nevertheless, due to the variability and intermittent nature of the wind and the operational restrictions of the wind turbines (they are stopped if the wind speed is below the cut-in wind speed or above the cut-out wind speed value), WECs could play an important role as auxiliary power suppliers, thanks to their contribution during the disconnection times of the wind turbines. This way, the efficiency of the far offshore hybrid farm could be importantly improved with respect to an energy farm based solely on wind, thus reducing the Levelised Cost of Energy (LCOE).

The wind and wave energy resources in the Atlantic ocean have been analysed using *ERA5* [35], which is a widely-used tool for the study of renewable energy resource data in locations worldwide [36]. In fact, many studies assessing the energy resource at different locations can be found in the literature: Meteorological measurements and wave resource data obtained with a buoy in the Icelandic Sea [37], a detailed analysis of the wave energy resource along the coast of Santa Catalina in Brazil [38], a study of the wave and tidal energy resource of the shelf seas in Uruguay [39] or the hybrid wind-wave energy resource in the northwest coast of the Iberian Peninsula [40] to name a few.

Previous evidence suggest that the large-scale teleconnection patterns affect the interannual variability of the wave height [41], the mean wave period and direction [42] and the available wave energy [43] at the regional level computed by means of regression analyses. Thus, the results from these studies will be compared with the ones obtained in this article using an alternative technique. The performance and subsequent hydrogen production of different sized WECs is calculated in the present analysis by considering realistic meteorological data and its covariance with the wave energy flux over the Atlantic. Hence, the contribution of the wave energy to improve the efficiency of a far offshore hybrid wind-wave energy farm can be assessed in a convenient way. As a result of the comparison of the performance of different WECs in this study, a more complex methodology for the selection of an optimal WEC in a defined location could arise, considering not only the generated auxiliary hydrogen, but also the size and the mass of the WEC and their affection in the integrity of the far offshore floating platform and its mechanical loads.

The modelling and simulation of the motion of the WEC, considering the displacement constraints and maximum force of the generic PTO system, has been accomplished by means of the open source Matlab toolbox WecOptTool [44], which allows to conduct simulations of a WEC at different sea states with high precision. Additionally, the hydrodynamic parameters of the designed oscillating bodies are obtained via simulations with the Boundary Element Method (BEM) code NEMOH [45], which is a consolidated and highly extended tool for the computation of hydrodynamic parameters of offshore structures. As the present analysis deals with an energy assessment, the selection of the mooring technology is considered to be out of the scope. Likewise, a generic PTO is considered, which could be implemented in the real device either as an hydraulic or as an electrical system.

This paper is structured as follows: In Section 2 the wind and wave energy resource data obtained with *ERA5*, the analysis method based on the covariance and a detailed explanation of the design, modelling and simulation of the WEC are given. In Section 3 and Section 4, the results and the discussion are presented, respectively. Finally, the conclusions of the conducted analysis are explained in Section 5, including an initial assessment of the predictibility of the total wind plus wave energy production.

2. Methods

This section is organised as follows: In SubSection 2.1 the procedure to obtain the wind and wave resource data with *ERA5* is presented. The theoretical basis of the Maximum Covariance Analysis (MCA) is presented in SubSection 2.2. The WECs considered for the calculations are presented in SubSection 2.4. The normalization process for the presentation of the obtained results is explained in SubSection 2.5.

2.1. Data

Hourly-averaged Wind Power Density (WPD) and magnitude of Wave Energy Flux (WEF) values have been derived from *ERA5* Reanalysis [35] data over the North Atlantic. These data have been downloaded from the Copernicus Climate Change Service's Climate Data Store (CDS) for the 2010–2019 time period. First, zonal and meridional components of the wind at 10 m height, temperature and dew-point temperature at 2 m and pressure at the surface have been used to estimate the WPD, see Eq. (1). The wind speed data present an horizontal resolution of $0.25^\circ \times 0.25^\circ$ over the domain given by longitudes $\lambda \in [-80^\circ\text{E}, 20^\circ\text{E}]$ and latitudes $\varphi \in [30^\circ\text{N}, 70^\circ\text{N}]$. Moreover, from the hourly-averaged density, wind speed and WPD values, their seasonal averages have been calculated by considering December, January and February as winter; March, April and May as spring; June, July and August as summer and September, October and November as autumn. Finally, the daily averaged fields have also been computed for the analysis of covariability between WPD and WEF.

$$W = \frac{1}{2}\rho U^3 \left[Wm^{-2}\right] \tag{1}$$

Regarding ocean wave energy, the magnitude of WEF has been computed over the same region and period as WPD by using hourly data and considering the expression for deep water, see Eq. (2), where H_s is the significant wave height of combined wind and swell and $\overline{T}$ is the mean wave period. The wave data present an horizontal resolution of $0.5^\circ \times 0.5^\circ$. Additionally, in order to correlate with the power matrix presented in Fig. 8, the peak period has also been downloaded from the *ERA5* wave model. Finally, the hourly values of WEF, the significant wave height H_s and the mean wave period $\overline{T}$ have also been seasonally averaged for diagnosis of the WEF field, and daily averages have been computed for the study of the coupled WPD and WEF variability.

$$\left|\vec{F}\right| = 0.491 H_s^2 \overline{T} \left[kWm^{-1}\right] \tag{2}$$

The monthly values of the Artic Oscillation (AO) [46], the North Atlantic Oscillation (NAO) [47] and the East Atlantic pattern [48,49] covering the same period (2010–2019) have been downloaded from the Climate Prediction Center Web server.

2.2. Wind and Wave Maximum Covariance Analysis

The covariability of the WPD and the WEF has been studied by means of the MCA, following [50]. The MCA identifies the linear combinations of the original fields which lead to maximum covariance between temporal expansion coefficients computed from both fields' anomalies. In previous studies found in the literature, the MCA method has been used to determine the leading coupling modes between different variables: The significant wave height and the peak period and the significant wave height and the surface wind over the Southern Atlantic [51], the sea-surface temperature and the surface wind over the Tropical Pacific [52] and the sea-surface temperature and the wind stress over the Peruvian coasts [53].

In this study, the MCA has been applied to daily anomalies of the WPD (left field, following the description of the method in [50]) and the magnitude of WEF (right field). Since the analysis extends through a wide range of latitudes (from southern to northern areas of the domain), the values at every grid point have been scaled by multiplying them by the renormalizing factor $\sqrt{\cos\varphi}$, being φ the corresponding latitude, see [54]. This ensures that polar regions, which are characterized by a higher number of grid cells for the same area, do not get oversampled. Additionally, as the default value of the grid spacing recommended by the CDS for wind data (0.25°) and for wave data (0.5°) is not the same, the WPD fields have been reprojected onto the WEF grid by means of a nearest-neighbour algorithm.

Before the covariance matrices used in the MCA are calculated, the daily averages of the WPD and magnitude of WEF values are computed and standardized, since both variables are not expressed in the same units. This preprocessing is intended to avoid giving more weight to the field with the highest variability. Furthermore, the expected errors (sampling errors) in the singular values computed by means of the MCA analysis have been estimated by means of bootstrap [55]. To that end, random samples with 0.67 times the number of elements in the original sample have been extracted and, from these ones, an additional random resampling with repetition has been carried out to arrive to synthetic samples with the total length equal to the length of the whole sample. The process has been repeated 2000 times and a two-sided 95% confidence interval for the singular values has been calculated from the random samples.

Finally, an analysis of the relationship between the teleconnection indices and the temporal coefficients obtained from the MCA analysis has been carried out, by computing monthly averages of the temporal left and right MCA-based expansion coefficients. The seasonal cycle in these expansion coefficients has been removed and the correlation between the expansion coefficients' monthly anomalies and monthly indices (anomalies themselves) has been computed, thus calculating the fraction of variance (R^2) explained by every linear model used. Those relations, described in SubSection 3.1, present a confidence higher than 95% of not being random according to a significance test. As some of the expansion coefficients and the data show significant low-frequency variability (seasonal cycle), this significance test is run by generating 1000 autoregressive AR1 random sequences with the same autocorrelation and standard deviation of the error term as the ones in the expansion coefficients and every WPD and WEF grid point.

2.3. Existing wave-wind co-located far offshore systems

Although Babarit et al. [16] cite several possible technologies for the production of far offshore wind energy and although this paper is basically a resource assessment study, the technological combination of wind energy with wave energy should be briefly analyzed for far offshore applications.

First, it should be mentioned that the analysis presented in this paper is intended for co-located farms, because the wave weakening due to the presence of WECs is not considered for the corresponding stability of the floating wind turbines [56]. Considering this beneficial interaction of wave energy absorption for wind energy production, an hybrid system, such as Poseidon Floating Power by the Netherlands' Floating Power Plant AS [57] or W2 Power, proposed by Pelagic Power AS [58], could be paradigmatic approximations of hybrid systems to which the present analysis is intended, see Fig. 1 for the first case.

This kind of hybrid co-located systems should, however, be adapted for far offshore applications. Floating islands can be a solution. These structures are large floating multipurpose platforms, where a combined harnessing of marine resources can be carried out, not only wave-wind based energy production. The 50 MW platform project proposed by the UK's Energy Island Ltd. is an example [56], as well as the sailing wind

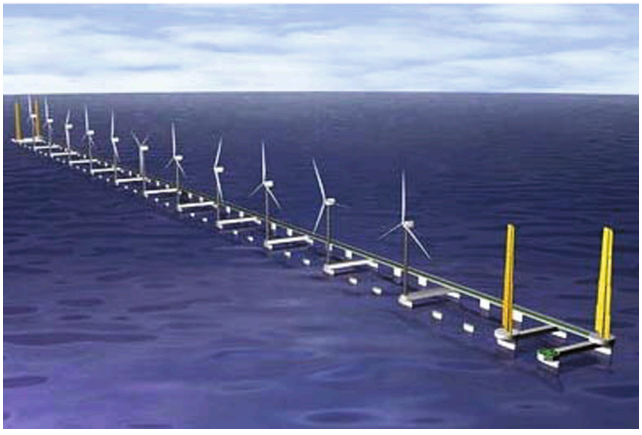

Fig. 2. Graphical illustration of a sailing wind farm proposal by [59].

Fig. 1. Poseidon Floating Power, by the Netherlands' Floating Power Plant AS [57].

farm proposed by Tsujimoto et al. [59], in which an array of simple point absorbers can be implemented, see Fig. 2. This sailing wind farm is composed of a semi-submersible floating structure, eleven windmills, four sails and a storage for hydrogen, which perfectly fulfils the perspective of the present study. Furthermore, an effective meteorological model to search for optimum marine routes was developed, the path of which can reach far offshore locations around Japan, respecting the water limits established by Mariana Islands, Marshal Islands, Micronesia and Russian Federation within approximately 300 km [59]. The installation of wave energy arrays constituted of simple point absorbers in these kind of sailed semi-submergible systems with several wind turbines seems to be a suitable technological approach for the far offshore resource assessment study proposed in this paper.

Regarding the survival of these far offshore structures, the construction, operation and management of floating oil rigs constitutes a referential industrial experience. For instance, Perdido oil rig in the Gulf of Mexico is about 300 km away from the coast and is moored in approximately 2400 m of ocean water [60]. In any case, the proposal of a specific technology for a far offshore hybrid wind/wave energy co-located farm is out of the scope of this work, in which the main contribution is based on the pioneering application of MCA to identify the optimum combination of both marine renewable energies, together with the analysis of various WEC geometries for the optimal production of hydrogen.

2.4. Wave Energy Converter

A two body point absorber oscillating in heave has been considered as the reference WEC in this analysis. The geometry of the designed oscillating body is based on the shape of the Reference Model 3 (RM3) point absorber, see Fig. 3a. The RM3 is a reference device created by Sandia National Laboratories and financed by the Department of Energy of the United States, with the objective of developing an open-source code and methodology aimed to the design and analysis of Marine HydroKinetic (MHK) technologies.

Analog to the RM3 device, the reference WEC considered in this analysis is formed by two bodies: a floating surface buoy that oscillates in heave as a result of the excitation force induced by the waves and a submerged reaction plate. Additionally, there is a vertical column that connects the surface buoy with the reaction plate. The main objective of the reaction plate is to help damp the oscillations of the floating body. Furthermore, it is also used for the mooring of the point absorber, in order to keep its horizontal position fixed and avoid big translational motions of the device. Many studies analyzing the different mooring possibilities applicable to an in heave oscillating point absorber [61] can be found in the literature. In the present paper, the design of the mooring system of the device is considered to be beyond of the scope of the conducted analysis.

The main physical characteristics and operational constraints of the reference point absorber considered in this paper, from now addressed as *WEC 1*, are listed in Table 1. The performance and power capture of a WEC are directly related to the hydrodynamic forces induced by the incoming waves in both the floating and submerged body of the point absorber. Having defined the geometry of the reference point absorber *WEC 1*, see Table 1, the open source code NEMOH has been used to calculate its hydrodynamic parameters. NEMOH [45] is an open source code developed by the Ecole Centrale de Nantes. It is intended to calculate the first order loads on offshore devices due to their interaction with waves. As a result, this code can be effectively used to calculate the hydrodynamic parameters of point absorbers, which will define their performance and, thus, their power absorption. In this case, the definition of the mesh for the calculations of the hydrodynamic parameters associated to the reference *WEC 1* is shown in Fig. 3(b).

The WEC Design Optimization Matlab Toolbox (WecOptTool) [44] has been used in the present paper for the analysis of the performance of the two body point absorber. WecOptTool, devoloped by Sandia National Laboratories, is an open source code intended to carry out frequency-dependent performance analyses and optimization studies of WEC devices, including control strategies of different nature and considering the actuation constraints of the PTO system. A demonstration of the application of the WecOptTool to the frequency-dependent analysis of a WaveBot WEC is presented in the work by Coe et al. [62]. The consideration of the frequency-dependent dynamics of the

Table 1
Physical parameters and operational constraints of the reference point absorber - *WEC 1*.

Reference point absorber - *WEC 1*			
Physical characteristics			
Description	**Parameter**	**Unit**	**Value**
Radius of the surface buoy	R_1	m	4.5
Thickness of the surface buoy	h_1	m	2.25
Mass of the surface buoy	m_1	kg	73025
Radius of the reaction plate	R_2	m	7
Thickness of the reaction plate	h_2	m	1.125
Mass of the reaction plate	m_2	kg	157070
Height of the point absorber	h	m	12
Operational constraints			
Description	**Parameter**	**Unit**	**Value**
Maximum in heave displacement	z_{max}	m	7
Maximum PTO force	f_{PTOmax}	kN	15

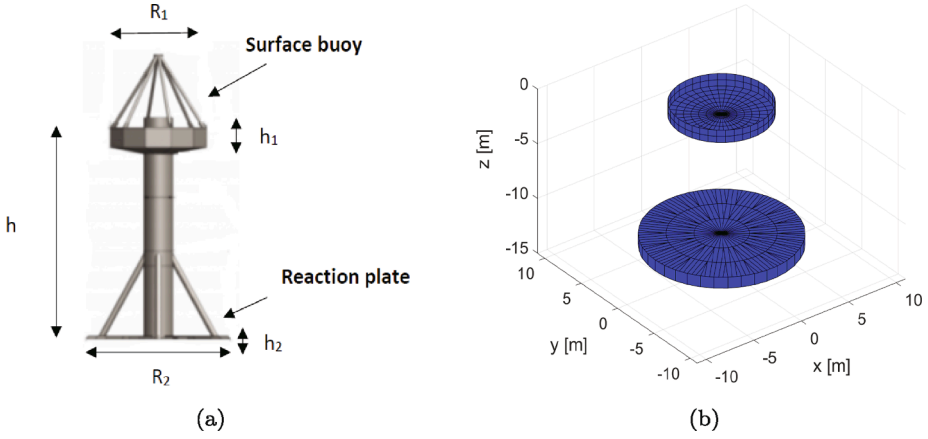

Fig. 3. (a) Geometry of the reference RM3 point absorber. (b) Mesh applied for the hydrodynamic analysis of the reference *WEC 1* point absorber.

point absorber is essential to conduct a realistic analysis, since the excitation forces induced by the waves and the response of the device do not relate linearly for the whole frequency spectrum of the waves.

Regarding the control strategy of the WEC (aimed to regulate the performance of the point absorber), a PseudoSpectral (PS) control strategy has been selected in this paper, applied by a generic PTO system. The PS controller [62] is based on the resolution of an optimization problem, in which the dynamics of the point absorber model, the motion of the WEC and the constraints corresponding to the maximum in heave displacement z_{max} and maximum PTO force f_{PTOmax} are considered. The objective of the optimization problem is to maximize the power absorption of the WEC, while not exceeding the performance constraints.

Hence, in this analysis, WecOptTool is used to model the performance of the designed WECs in variable but realistic wave resource conditions. The final objective is to estimate the power generation of the WECs in each one of the wave resource conditions, defined by the significant height H_s and the peak period T_p.

2.5. Normalization of Wave Energy according to Wind Energy

The power production of a floating offshore wind turbine is, in most cases, considerably larger than the one produced by a WEC, especially in far offshore applications, where the wind turbines are not subject to noise, transport or visual limitations. However, wind turbines are also susceptible to have disconnection times during their productive lives, as they might suffer from discontinuities due to the variability of the wind or maintenance tasks due to malfunctions of the wind turbine. Consequently, in the analysis conducted in this paper, the hydrogen production of variable sized WECs during the stopping time of far offshore wind turbines is to be computed and analyzed. In such cases, this hydrogen production is considered as additional and auxiliary, since it will improve the overall efficiency of the far offshore co-located wind-wave energy farm and help cover the energetic needs of the farm while the main wind based energetic generators are stopped. In the present analysis, the stopping times of the wind turbines due to mechanical issues are not considered, on account of the difficulty in their prediction without real operational data and the variability between individual wind turbines of the same model.

The Hywind National Renewable Energies Laboratory (NREL) 5 MW floating Horizontal Axis Wind Turbine (HAWT) [63] has been considered as the reference wind turbine in the present study. Based on the power production of the NREL 5 MW wind turbine, different WEC configurations are considered and described according to the normalized ratio of their maximum power generation value with respect to the rated power of the NREL 5 MW wind turbine. For instance, a WEC with 50 kW maximum power generation is to be characterized as a 1% power ratio WEC. Following this criteria, three WEC models with different size and power ratio are defined and listed in Table 2.

The design and simulation of the three different WEC models has been accomplished following the methodology described in SubSection 2.4. The corresponding meshes for the resolution of the hydrodynamic calculations of the variable sized WECs are presented in Fig. 4a and Fig. 4b, respectively. In comparison to the reference *WEC 1*, see Fig. 3b, the dimensions of the *WEC 2* have been increased, while the dimensions of the *WEC 3* have been reduced. The increase in the dimensions of the *WEC 2* will cause an increment of its mass, while the mass of the *WEC 3* will be reduced. Moreover, if the dimensions and the mass of a WEC increase, the force necessary to regulate its oscillation will have to be larger as well. Thus, in order to maintain the performance standards of the PTO control system in each one of the designed WEC models, the maximum force f_{PTOmax} must be adapted accordingly, as seen in Table 2. As a result, the correct performance of the PTO control system is ensured for all three models, and a realistic comparison is conducted. It must be noted that an increase of force of the PTO system will cause an increment of its cost and dimensions.

Table 2
Designed WEC models with different size and normalized power ratio.

	WEC models				
	R_1	R_2	M	f_{PTOmax}	*PowerRatio*
WEC 1	4.5 m	7 m	230095 kg	15 *kN*	1.76%
WEC 2	7 m	10 m	497250 kg	25 *kN*	2.16%
WEC 3	2 m	4 m	65712 kg	5 *kN*	0.86%

3. Results

This section is organised as follows: In SubSection 3.1 the results associated to the selection of the optimal locations after the MCA are presented. The power matrix and hydrogen generation of the reference *WEC 1* are presented in SubSection 3.2. The combined and normalized wind and wave hydrogen generation results are presented in SubSection 3.3.

3.1. Identification of locations. Maximum covariance analysis.

The selection of a sample of some of the most suitable locations in the Atlantic ocean for a far offshore co-located wind and wave energy farm has been performed according to the far offshore site evaluation criteria introduced in SubSection 2.2, in combination with the wind and wave resource data obtained through the meteorological analysis presented in SubSection 2.1. Following these evaluation criteria, four locations, marked with red circles in Fig. 5a, have been selected. The distance to the closest coast has also been shown in this Figure in order to focus on points very far from coast (P-00 and P-01 beyond 1000 km), a point not so far (P-02, close to 750 km from the nearest shore) and a closer one (P-03, around 500 km from the nearest coast). It should be emphasized that the Island of Azores constitutes a central geographical point that permits an almost total areal exploitation of far offshore marine renewable energy for the area of the North Atlantic.

The selection of the locations has been carried out on the basis of the results of the MCA analysis of the WPD and the WEF fields. The fraction of covariance between the WPD and the WEF fields over the Atlantic basin explained by each of the spatial modes identified in the MCA analysis is shown in Fig. 5b. The red or blue vertical lines represent the 95% confidence interval on the covariance fraction explained by each mode derived from the bootstrap analysis. The red colour indicates that the error bar does not overlap with the one corresponding to the next mode, while the blue colour indicates that overlapping (and therefore, sampling degeneracy) appears. Therefore, the leading mode represents a 79% of the common covariance, the second mode a 8% and the third one a 4%, which yields a 91% of total covariance explained by just three modes.

The spatial modes obtained from the MCA analysis are represented as homogeneous correlation maps [50] in Fig. 6. Points P-00 to P-03 have been selected under the criteria that they represent areas of high covariance. As shown in Fig. 6, P-00 and P-01 are located close to the maximum correlation areas in singular vector 1 both for left (WPD) and right (WEF) fields. However, the paper addresses the relevance of areas where the wave and wind energy are not that tightly coupled. To achieve this goal, P-02 and P-03 are selected at places with high absolute values of the correlation but negative signs, as shown by singular vector 2 (Fig. 6, middle row). Moreover, all of them are located relatively far from the continental coasts, so far that the installation of an energy farm would be considered as far offshore (>90 km).

Regarding the meaning of the main spatial modes identified in the MCA, the leading mode represents basically the seasonal cycle of storminess in the Atlantic, with the corresponding temporal expansion coefficients showing a highest amount of variability concentrated in periods longer than thirty days. The corresponding homogeneous correlation map for this leading mode (Fig. 6, top) shows that the seasonal

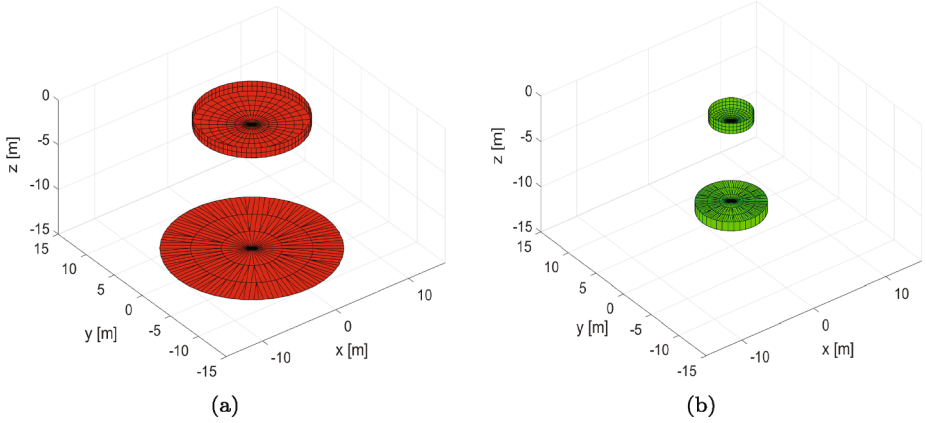

Fig. 4. (a) Mesh applied for the hydrodynamic analysis of the *WEC 2* point absorber. (b) Mesh applied for the hydrodynamic analysis of the *WEC 3* point absorber.

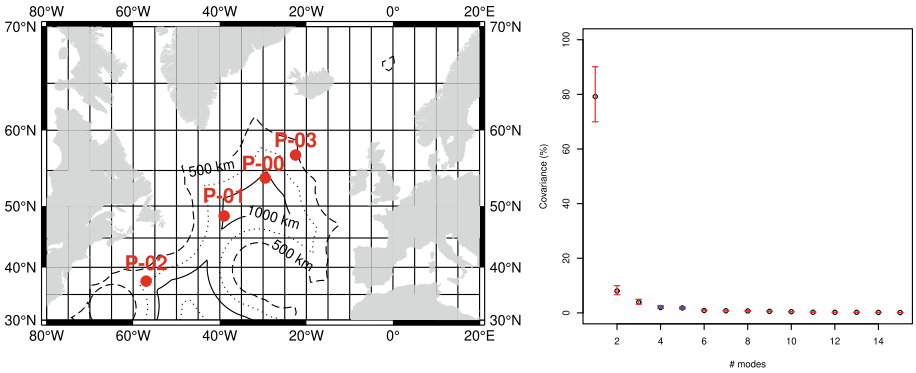

Fig. 5. (a) Study area and selected locations as identified from MCA. The contours represent lines of equal distance to the closest shore (km). (b) Fraction of covariance between WPD and magnitude of WEF as derived from MCA and corresponding error bars (95% confidence interval) computed by means of bootstrap analysis.

cycle affects with the same polarity every point in the North Atlantic basin, but it is most intense in central Atlantic areas.

On the other side, the second mode (Fig. 6, middle panels) represents a meridionally oriented dipole structure with positive correlations over northern areas and negative correlations over southern areas. The regression analysis of the monthly anomalies calculated from the temporal expansion coefficients for this second mode shows that it is tightly tied ($R^2 = 0.5$ for the WPD and $R^2 = 0.53$ for the WEF) with the AO [46] and less strongly ($R^2 = 0.36$ for the WPD and $R^2 = 0.33$ for the WEF) with the NAO [47].

Finally, the third mode (Fig. 6, bottom) shows alternate patterns of negative and positive spatial correlations over the Atlantic, with P-02 located at the highest negative correlation.

The monthly anomalies represented by the monthly averages of the MCA-based temporal expansion coefficients are affected both by the AO ($R^2 = 0.17$ for the WPD and the WEF) and ($R^2 = 0.21$ for the WPD and $R^2 = 0.18$ the WEF) by the East Atlantic [48,49] pattern.

3.2. Power Matrix and Hydrogen Production of the reference WEC 1

The temporal performance of the reference *WEC 1* point absorber with a wave elevation input defined by the significant height $H_s = 6.5$ m and the peak period $T_p = 3.5$ s during a time interval of 30 s is shown in Fig. 7. The upper plot represents the wave elevation η and the in heave motion of the point absorber z. The upper middle plot shows the motion velocity of the point absorber $\dot{z}$. The lower middle plot presents the instantaneous force exerted by the PTO system f_{PTO}. And, finally, the lower plot represents the instantaneous power generated by the WEC P.

The most computationally efficient way to convert long periods of energy resource data into generated power is using the power curve or power matrix of the corresponding energy converter. In such a matrix, the characteristics of the energy resource and the power generated by the converter are directly related, and thus, the performance of the converter gets fully characterized and its energy production over long temporal periods can be analyzed, avoiding the execution of a huge number of simulations. In this case, the frequency-dependent *WEC 1* model described in SubSection 2.4 has been simulated over its whole range of operating conditions, defined by the significant height H_s and the peak period T_p of the incoming waves, and the power matrix have been calculated. The power matrix of the reference *WEC 1* is shown in Fig. 8. The cut-in and cut-off significant wave heights in order to start and pause the production of the WEC have been set to 0.5 m and 6.5 m, respectively. Regarding the peak period T_p, simulations have been restricted to the interval between 0.5 s and 14 s, being the power absorption of the WEC for peak periods outside this range considered negligible. The obtained power matrix is observed to be in line with similar analyses found in the literature [64].

Once the performance of the point absorber has been characterized and the power matrix of the reference *WEC 1* calculated, the hydrogen generation that would result from the installation of this device in a far offshore energy farm located at the Atlantic ocean points defined in SubSection 3.1 has been computed. The main characteristics of the wind and wave energy resources at each one of these four locations is summarized in Table 3.

The energy generated by the reference *WEC 1* point absorber at each one of the locations has been computed by interpolation of the power matrix, see Fig. 8, with the wave resource data obtained in SubSection 3.1. For the hydrogen production, an energy consumption of 4.2 kWh

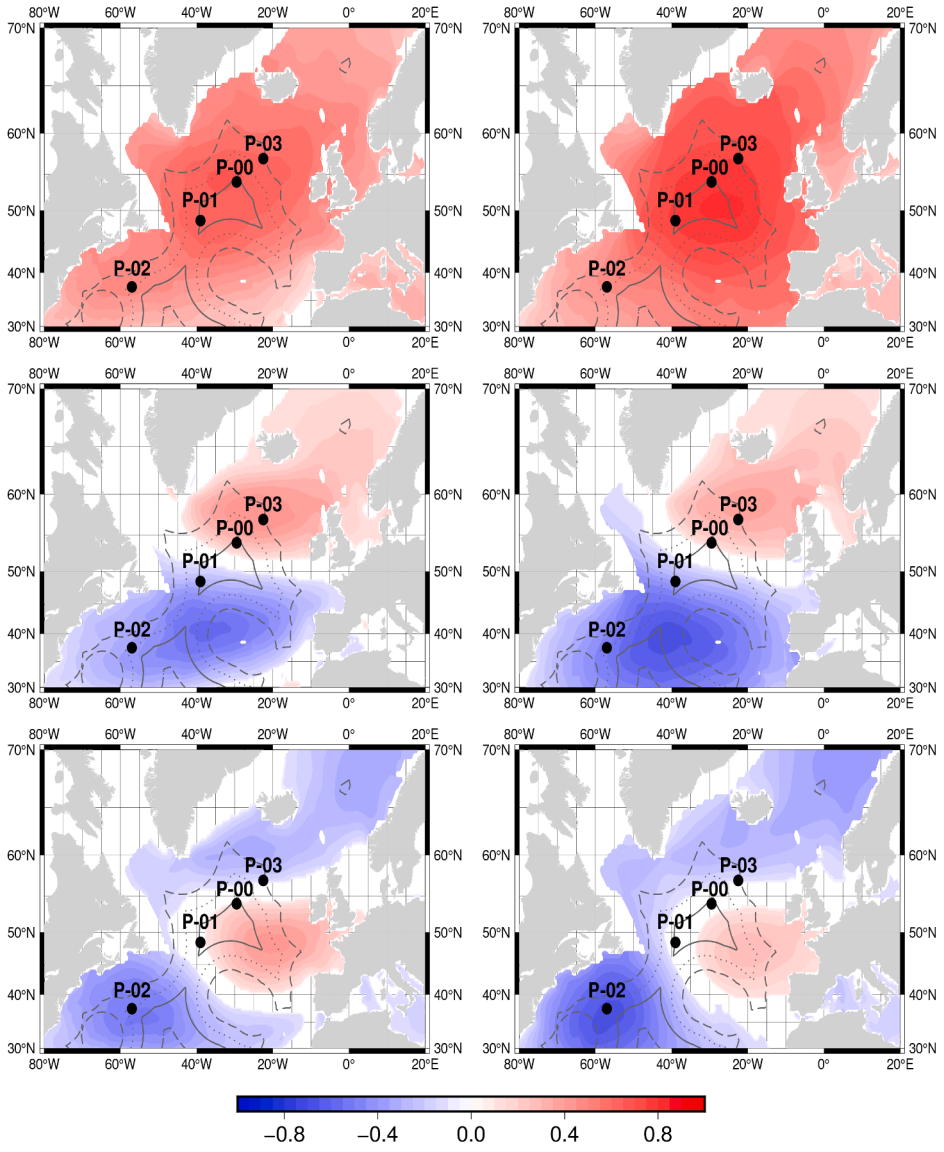

Fig. 6. Homogeneous correlation maps of MCA expansion coefficients with WPD (left, adimensional) and WEF (right, adimensional), from MCA modes (singular vectors) 1 (top), 2 (middle) and 3 (bottom). Grey contours represent distance to the nearest coastal point. The color scale represents the pointwise Pearson correlation coefficient between the left (WPD) or right (magnitude of WEF) fields with the temporal expansion coefficients corresponding to the first, second or third modes.

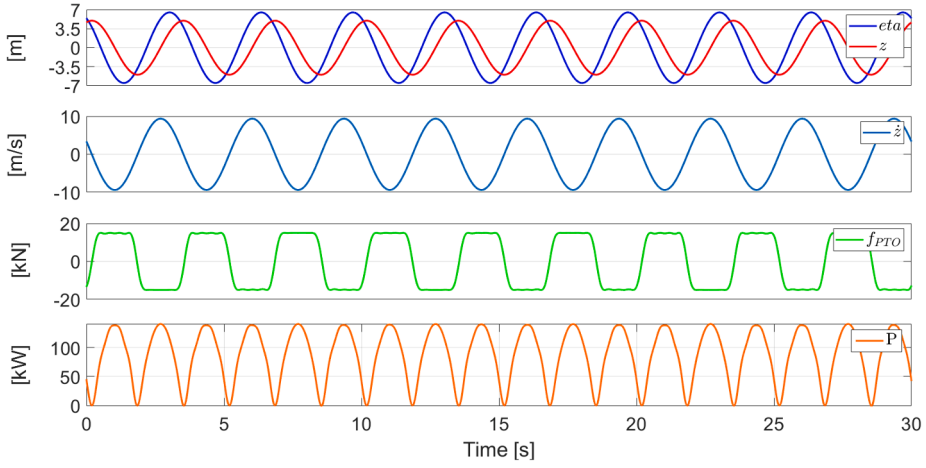

Fig. 7. Temporal performance of the reference *WEC 1* point absorber with waves defined by $H_s = 6.5$ m and $T_p = 3.5$ s.

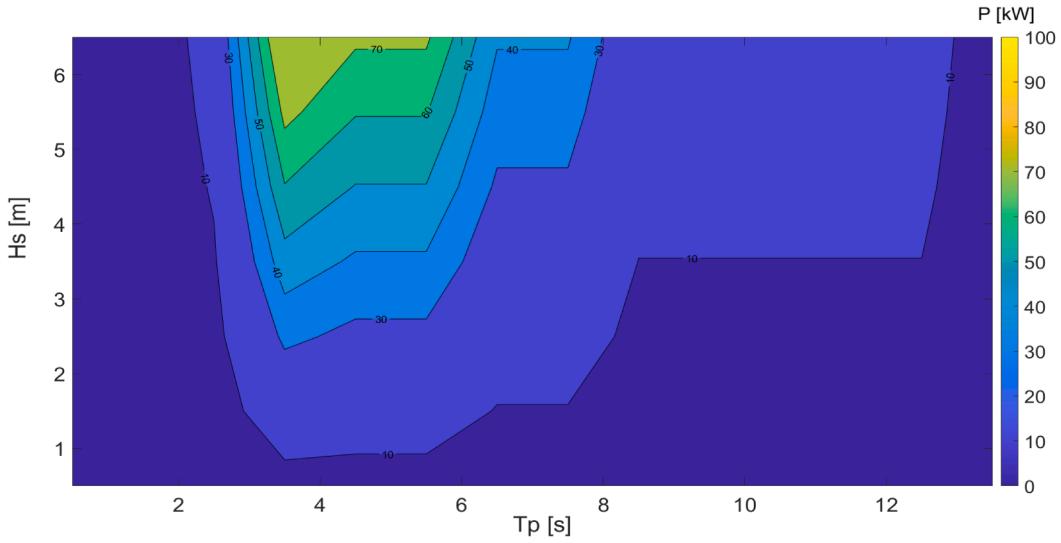

Fig. 8. Power matrix [kW] of the reference *WEC 1* point absorber.

Table 3
Statistical characteristics of the wind and wave energy resources at the selected Atlantic ocean far offshore locations.

	Significant wave height [m]				Peak period of waves [s]			
Point	**Max**	**Min**	**Mean**	**Std. Dev.**	**Max**	**Min**	**Mean**	**Std. Dev.**
P-00	14.61	0.69	3.49	1.69	13.62	3.53	6.85	1.41
P-01	17.66	0.63	3.5	1.7	3.49	12.7	6.75	1.34
P-02	11.82	0.64	2.67	1.36	11	3.3	6	1.22
P-03	15.45	0.67	3.52	1.75	13.15	3.4	6.84	1.41

	Wind speed [m/s]			
Point	**Max**	**Min**	**Mean**	**Std. Dev.**
P-00	32.91	0.05	9.83	4.19
P-01	30.75	0.06	10.03	4.36
P-02	28.95	0.03	8.75	3.96
P-03	29.1	0.08	9.89	4.36

Nm^{-3} has been considered. This global energy consumption is itemized in detail in the work of Saenz-Aguirre et al. [65], where the global efficiency and energy consumption of a wave energy based offshore hydrogen production system are calculated. The global efficiency includes the individual efficiencies of the desalination, compression, electrolysis and additional processes. Using this energy consumption

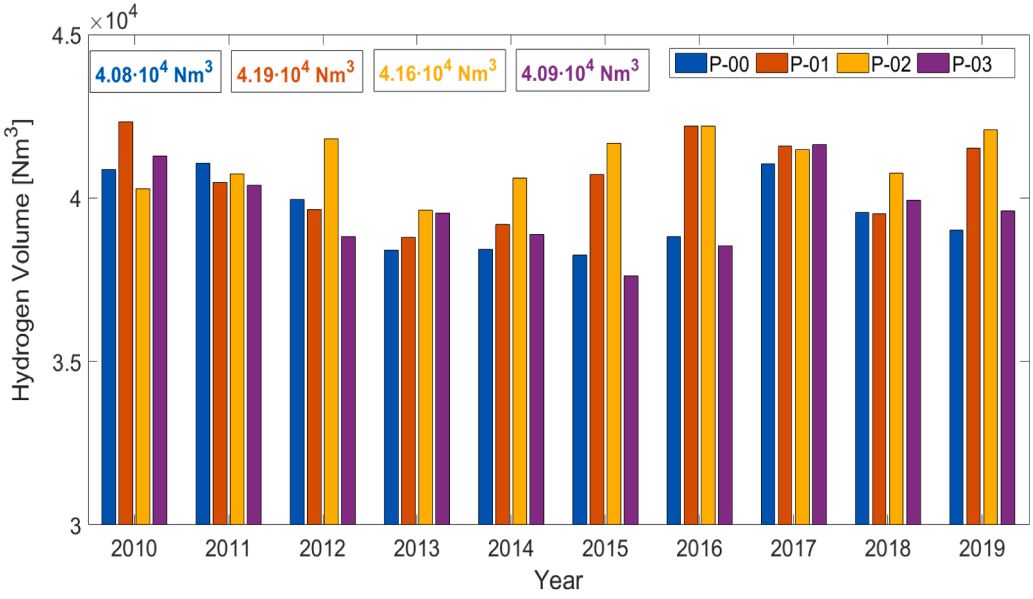

Fig. 9. Hydrogen generation $[Nm^3]$ of the reference *WEC 1* point absorber at the selected North Atlantic locations.

value, the hydrogen volume generated by the *WEC 1* point absorber at each one of the four selected locations and for the last ten years is presented in Fig. 9.

The yearly hydrogen production of the reference *WEC 1* shows a rather constant tendency and limited variability between productions values at one same location. A maximum production variability of 8.91% is found at location P-03 between years 2015 and 2017. For the rest of the locations, maximum variabilities of 7.36%, 6.83% and 7.29% have been found in P-00, P-01 and P-02, respectively. As a result, the uniformity of the wave resource trend emphasizes the important contribution a WEC could make as an energy/hydrogen supplier in a far offshore hybrid wind and wave energy farm.

Regarding mean hydrogen production of the *WEC 1*, the highest generation volume is found at location P-02. Correlating the statistical wave resource data in Table 3 and the power matrix in Fig. 8, it can be observed that although the mean significant height H_s of the wave resource in the location P-02 presents the lowest value, the maximum hydrogen production is achieved. The reason for that is that the mean peak period T_p of the wave resource in the location P-02 is the closest to the value of maximum power absorption of the WEC, as it can be observed in Fig. 8. In fact, it presents the lowest mean value and the lowest standard deviation from all studied locations. Therefore, the hydrogen production is maximal in P-02. The location with the minimum hydrogen production is P-00, where the mean significant height H_s of the waves is high, but the mean peak period T_p is the highest.

3.3. Combined and Normalized Wind and Wave Hydrogen Generation

In order to get an accurate idea of the efficiency of a WEC in comparison to a wind turbine located in the same far offshore energy farm, the wave energy based hydrogen production is normalized in this Subsection with respect to the wind energy based hydrogen production. Three different analysis scenarios have been considered, each one corresponding to a WEC model listed in Table 2 (*WEC 1*, *WEC 2* and *WEC 3*). Following the methodology in SubSection 3.2, the power matrices corresponding to the devices *WEC 2* and *WEC 3* have been calculated and are presented in Fig. 10a and Fig. 10b, respectively.

By comparing the power matrices corresponding to *WEC 2* and *WEC 3*, it is evident that, as expected, the power absorption/production of the WEC increases when incrementing its dimensions. As a result, the power matrix of the point absorber *WEC 2* shows remarkably larger values than the one of the point absorber *WEC 3*. Additionally, it is observed that by incrementing the dimensions of the WEC, the peak period T_p corresponding to the maximum power absorption of the WEC is shifted to higher values, which results in a higher power absorption of the *WEC 2* at greater values of the peak period T_p. Due to the characteristic peak period T_p of the wave resource at each location, the dimension of the WEC will determine its power absorption, and hence suitability, for that specific location.

For the calculation of the normalized hydrogen production, a 5/1 relation has been considered in the number of wave converters with respect to the number of wind turbines in all scenarios, i.e, five WECs have been considered for each wind turbine in the farm. Following the methodology described in SubSection 3.2, the hydrogen volume production has been calculated for each one of the three scenarios and the four far offshore locations selected with the MCA analysis. In addition, the produced total hydrogen volume has been divided with respect to its origin: wind energy based (produced with the power absorbed by the NREL 5 MW wind turbine) or wave energy based (produced with the power absorbed by the corresponding WEC). Subsequently, the normalized mass (with respect to the reference *WEC 1*) and the normalized hydrogen production of each one of the WEC scenarios at the four far offshore locations have been calculated and are represented in Fig. 11.

A summary of the hydrogen produced by the NREL 5 MW wind turbine and the normalized WEC based hydrogen production is presented in Table 4.

The results presented in Table 4 show that important additional hydrogen volumes can be achieved in a far offshore wind farm by installation of WECs. As expected after the results in SubSection 3.2, the highest hydrogen production volumes have been found at location P-02, where five WECs of the type *WEC 1* could supply a 4.03% of the hydrogen produced by the NREL 5 MW wind turbine during the last 10 years. The lowest additional hydrogen volume production would result at location P-00, where a 3.32% of the hydrogen produced by the HAWT would be supplied by five WECs of the type *WEC 1*.

In case of the *WEC 2* point absorber, a maximum additional hydrogen production of 6.28% is achieved at location P-02. However, this is

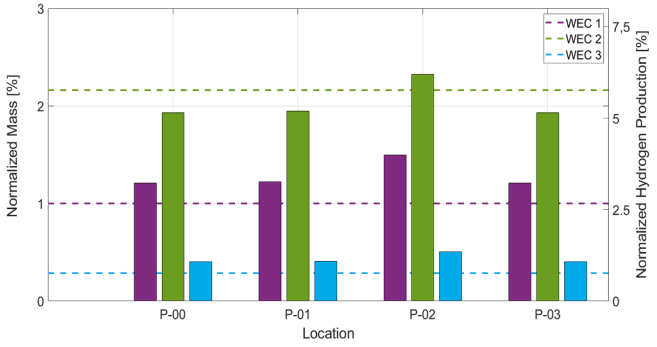

Fig. 11. Normalized mass (dashed lines) and hydrogen production (bars) of the different sized WEC configurations at the selected far offshore locations.

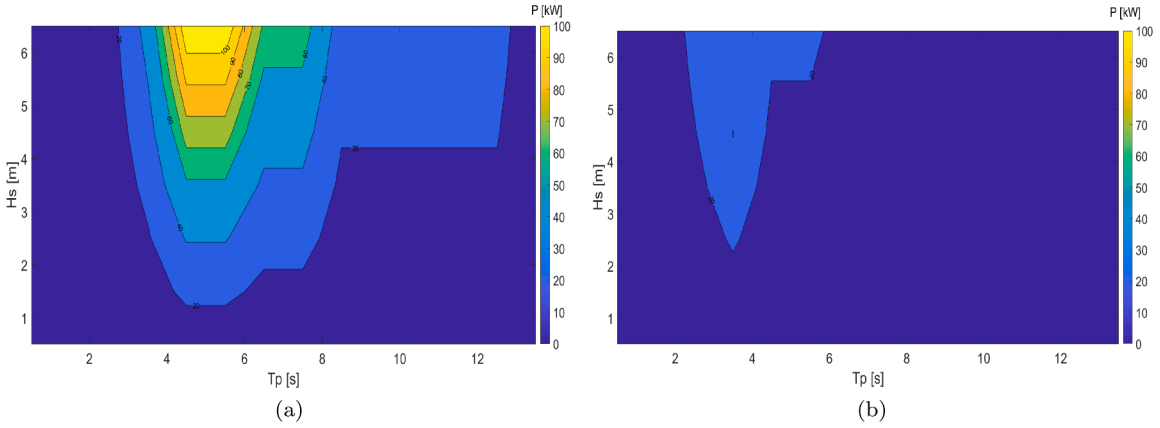

Fig. 10. (a) Power matrix [kW] of the *WEC 2* point absorber. (b) Power matrix [kW] of the *WEC 3* point absorber.

Table 4
Hydrogen produced by the HAWT and normalized hydrogen production of the different WEC scenarios.

	Point P-00			Point P-01		
HAWT H_2	$6.14{\cdot}10^7$ Nm^3			$6.24{\cdot}10^7$ Nm^3		
	WEC 1	**WEC 2**	**WEC 3**	**WEC 1**	**WEC 2**	**WEC 3**
WEC H_2	3.32 %	5.32 %	1.11 %	3.36 %	5.38 %	1.12 %
	Point P-02			**Point P-03**		
HAWT H_2	$5.16{\cdot}10^7$ Nm^3			$6.15{\cdot}10^7$ Nm^3		
	WEC 1	**WEC 2**	**WEC 3**	**WEC 1**	**WEC 2**	**WEC 3**
WEC H_2	4.03 %	6.28 %	1.36 %	3.33 %	5.32 %	1.11 %

accomplished by increasing the mass of the WEC in a 1.16 %, see Fig. 11, which will cause an increment of the cost of the WEC, the PTO system and the mooring to the offshore platform. Regarding *WEC 3*, a maximum additional hydrogen production of 1.36% is achieved at location P-02. In this case, the mass of the WEC is reduced in a 0.72%. It is to be observed that the maximum difference between the various WEC configurations can also be found at location P-02. The increase in the mass of the *WEC 2* causes a shift of its period of maximum absorption towards higher values, i.e. closer to the mean wave peak period at location P-02. As a result, its power production is maximized with respect to the other WEC configurations. This fact clearly stresses the importance of a WEC design procedure focused on the meteorological characteristics at a specific location.

Finally, the capacity of the WECs to provide auxiliary energy/hydrogen has also been analysed in this Subsection. To that end, the hydrogen production of the different WEC scenarios during the disconnection time of the NREL 5 MW wind turbine in the corresponding far offshore location is presented in Table 5. In order to compute the stopping time of the HAWT, the wind speed data obtained in SubSection 3.1 (and statistically summarized in Table 3) has been analyzed to find the wind speed values below the cut-in (3 m/s) or above the cut-off (25 m/s) wind speed values that define the operation range of this wind turbine. Due to the lack of operational data of a real offshore wind turbine, the disconnection times as a result of maintenance and mechanical issues are not taken into account. Regarding the maximum admissible wave elevation for the disconnection of the NREL 5 MW floating wind turbine, this value is bigger than the cut-off wave elevation for the proposed WECs. Therehore, no auxiliary hydrogen could be produced by the WECs if the wind turbine would be stopped due to too high wave elevation.

According to the results of the MCA presented in SubSection 3.1, the wind and wave energy are highly coupled in the locations P-00 and P-01,

Table 5
Auxiliary hydrogen production of the different WEC scenarios in the selected far offshore locations.

	Point P-00			Point P-01		
HAWT stop	3780 h			3820 h		
	WEC 1	**WEC 2**	**WEC 3**	**WEC 1**	**WEC 2**	**WEC 3**
Auxiliar H_2	50073 Nm^3	82129 Nm^3	16646 Nm^3	52374 Nm^3	85754 Nm^3	17408 Nm^3
Eq. HAWT	42.06 h	68.99 h	13.98 h	43.99 h	72.03 h	14.62 h
	Point P-02			**Point P-03**		
HAWT stop	5652 h			4317 h		
	WEC 1	**WEC 2**	**WEC 3**	**WEC 1**	**WEC 2**	**WEC 3**
Auxiliar H_2	75133 Nm^3	120380 Nm^3	24963 Nm^3	56925 Nm^3	93094 Nm^3	18930 Nm^3
Eq. HAWT	63.11 h	101.12 h	20.97 h	47.82 h	78.2 h	15.9 h

but this coupling is weaker at locations P-02 and P-03. As it can be observed in Table 4, the normalized mean hydrogen production of the WECs do not show a considerable dependency on the coupling between the wind and wave energy in the particular far offshore location, see very similar production values at locations P-00, P-01 and P-02. Instead, the peak period T_p of the wave resource has been found to be the most influential parameter for a maximized hydrogen production.

Nevertheless, according to the results provided in Table 5, the coupling between the wind and wave energy is an important factor to be considered when analysing the auxiliary hydrogen production of a WEC. In those locations where the coupling between the WPD and the WEF is weaker, the number of hours in which the wind turbine is stopped, but the wave resource characteristics are adequate to produce, are greater. As a result, the auxiliary hydrogen production of the WECs become more important and the significance of their role maximized. As it can observed in Table 4, out of the total disconnection time of the HAWT, 101.12 h of equivalent operation of the HAWT (producing at 5 MW rated power) could be recovered with five WECs of the type *WEC 2* at location P-02. The maximum equivalent HAWT operation recovery hours found at locations P-00, P-01 and P-03 are 68.99 h, 72.03 h and 78.2 h, respectively.

4. Discussion

The fact that the expansion coefficients associated to the leading WPD/WEF coupled mode identified in the MCA analysis show a strong seasonal cycle, implies that their temporal behaviour allows a relatively easy predictability. Even for the second or third modes, see Fig. 12, in which the AutoCorrelation Function (ACF) decays much faster, there seems to exist some predictability based just on persistence up to 5 days (ACF>0.25) for the three modes which, as has already been indicated before, explain up to a 91% of the total covariance of daily WPD and WEF. The application of this result to the operational management of the kind of combined energy generation system analyzed in this paper is out of the scope of this paper, but future studies must build on the shape of these ACFs.

Some of the large-scale atmospheric teleconnection patterns, such as the NAO or the East Atlantic pattern, are well known for affecting atmospheric processes over the Northern Hemisphere and, in particular, its Atlantic basin [66]. Thus, it was expected from the beginning that their influence could be detected in the results presented in this contribution. However, it is found that they are affecting large fractions of the covariance between WPD and WEF over the whole basin.

The results in this paper, which link the spatial patterns of the MCA modes (homogeneous correlation maps shown in Fig. 6), through their corresponding expansion coefficients are in line with previous findings calculated by local regression of teleconnection indices onto wave energy flux at every grid point [42]. Some studies show that the available wave energy has already changed [67] over the Atlantic in the past and might also change in the future as a result of climate change, depending on the Representative Concentration Pathway followed by society [68]. Similarly, there are evidences of substantial variations in wind speed [69] and renewable energy produced in Europe [70]. Teleconnection patterns also affect temperature [71] which is a factor in the determination of WPD [72] and it is also changing due to global warming [73]. Thus, future studies should also be addressed to the coupling between WPD and WEF under future climate scenarios.

All in all, the coupling between the WPD and the WEF has been proven to be an important factor to be considered during the selection of the optimal location for far offshore hybrid wind and wave energy farms, where the variability of the wind speed, and the consequent disconnection times of the HAWTs, could lead to reduced energy/hydrogen generation for time intervals of uncertain duration, see the results in Table 5. During these time intervals, the auxiliary hydrogen produced by the WECs could help improve the efficiency of the farm and cover its energetic needs. Hence, the installation of WECs would result more

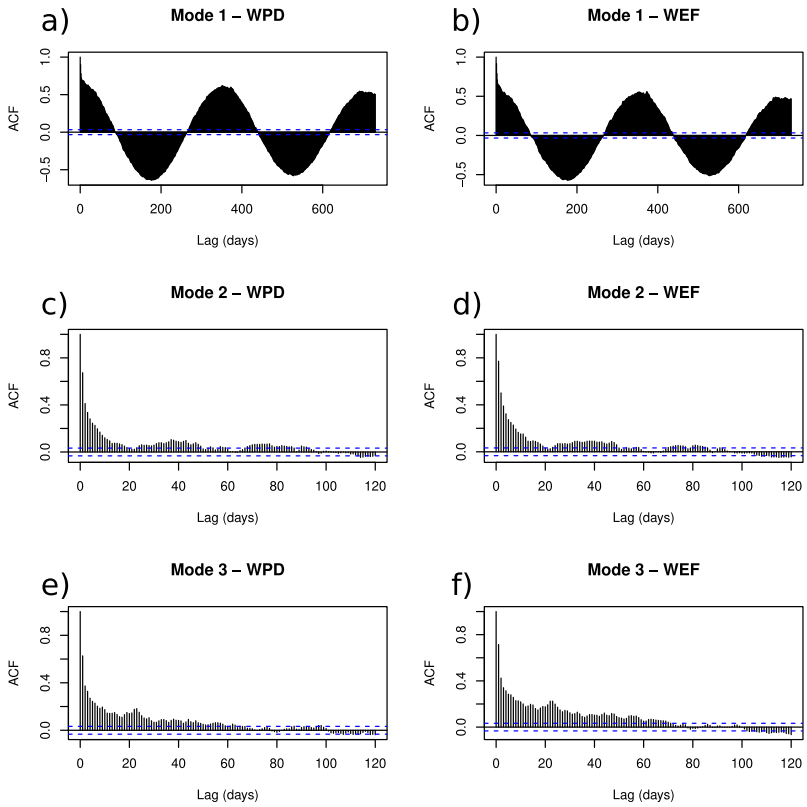

Fig. 12. Autocorrelation functions corresponding to the temporal expansion coefficients derived from the leading mode of WPD (top, left, panel a) and WEF (top, right, panel b), the second WPD mode (middle, left, panel c) and WEF (middle right, panel d). Finally, autocorrelation function for the third mode of WPD (bottom, left, panel e) and WEF (bottom, right, panel f).

essential in far offshore wind farms with high wind variability and low covariance between wind and waves.

The selection of the WEC model for a far offshore energy farm should be particularized with respect to the characteristics of the wave resource in the corresponding location. While WECs of larger dimensions have their maximum power absorption at higher peak period T_p values, WECs of lower dimensions absorb more power from wave resources with lower peak periods T_p values. As a result, the characteristics of the wave resource, and the influence of the large-scale teleconnection patters on them, should be taken into consideration in the desing process of the WEC to be installed in a far offshore energy farm. For instance, in a location with low significant height H_s and high peak period T_p values, a larger WEC should be installed. On the contrary, in a location with high significant height H_s and low peak period T_p values, a smaller WEC would be the best device to be installed.

In economical terms, the identification of the optimal locations for the installation of a hybrid farm enables to maximize the amount of generated energy/hydrogen. Thus, providing a qualitative economic estimation of the generation costs. Additionally, the dimensions of the WEC are an important factor to be taken into account as well, since they will directly affect the economical cost of the device and, indirectly, the design of the mooring system and the far offshore platform. Therefore, although in the present paper the design and dimensioning of the far offshore platform and the mooring system have been taken for granted, a more complex methodology for the selection of the optimal location of a far offshore farm could arise in future works. A methodology in which the characteristics of the wave resource in a given location and its influence on the economical cost of the platform and the mooring system are related. Thus, a comprehensive economic evaluation based on specific technological solutions could be carried out.

In this paper, hydrogen production has been considered as the procedure for energy storage in the far offshore hybrid farm. Nowadays, many governments and international companies are promoting the production of hydrogen with energy based on renewable energies and its use as a renewable fuel instead of classic fossil fuels. Among the technological developments that may contribute in the future to the development of far-offshore hydrogen production is the use of seawater for the electrolysis process instead of the current use of distilled water [74]. The European Union considers hydrogen a key element in the ongoing efforts towards a cleaner economy, among other things, because it is an area where Europe is still leading [75]. In recent studies, on account of the low volumetric energy density of the hydrogen (in standard conditions of temperature and pressure), the use of methanol is proposed for energy storage in energy ships [18]. According to these studies, many advantages are related to the use of methanol instead of hydrogen, such as, a good efficiency in the production, a high market value and its liquid state in standard temperature and pressure conditions. Consequently, the development of the methanol as the energy vector in far offshore applications must be in sight for future works related to this topic.

The results of this paper are aligned with some of the challenges identified by all the Member States of the United Nations in a Resolution by the General Assembly of the United Nations adopted on September 2015, commonly called the 2030 Agenda for sustainable development [76]. In this resolution, there were 17 main goals which were developed up to 169 different targets which addressed the need to achieve a sustainable development whilst, at the same time, erradicating poverty. In particular, Sustainable Development Goal (SDG onwards) number seven (SDG7) is devoted to ensuring access to affordable, reliable, sustainable and modern energy for all. This goal covers targets such as the need to increase the share of renewable energy, facilitate the access to renewable energy to the population or upgrade technology so that renewable energy can also be used in land-locked developing countries. The

findings presented here are expected to contribute in the future to these targets, because the area of ocean in which offshore wind energy can be produced is greatly expanded, so that geographical, spatial planning or other ocean uses are not so heavily affected by offshore wind farms [77]. Besides the use of renewable energy sources, the use of hydrogen as an energy vector is also considered by some authors as potentially leading to a better integration of renewable energies in the electricity sector [78], which agrees with the findings presented in this paper. However, as is also widely recognized in the literature, energy is a factor which affects different sustainability goals at the same time [79]. In the case of this paper, the increase in the efficiency of production of renewable energy affects the SDG13 (Take urgent action to combat climate change and its impacts) by improving the ability to reduce emissions from fossil fuels. The spatial planning implicit in the results presented allows a better planning in the use of renewable energy resources, which is the Target 13.2 in this SDG13. Finally, SDG14 (Conserve and sustainably use the oceans, seas and marine resources for sustainable development) includes some targets such as 14.7 (increase the economic benefits to small island developing states and least developed countries from the sustainable use of marine resources). An increased use of renewable energy sources has already been identified by previous studies [79] as a positive feedback in terms of SDG14 because the reduction of the carbon dioxide emissions will slow rates of ocean acidification. Beyond this, the authors foresee that small islands in the middle of the oceans can benefit from the ability to serve as points used for managing the kind of floating infrastructures presented in this paper. Previous studies also show that a sustainable use of ocean areas, the so called Blue Economy [80], improves indicators in SDG15 (sustainable use of terrestrial ecosystems), for instance, leading to a smaller footprint of terrestrial wind energy farms with less affections to mountain ecosystems or forests, by increasing the number of offshore installations. In any case, there might appear both synergies and incompatibilities when a full analysis of particular technologies are analyzed from the point of view of multiple Sustainable Development Goals. Thus, whilst the use of hydrogen as an energy vector will reduce emissions, it might lead to negative impacts depending on the technologies used in its production [78]. Systematic analyses of the interrelationships which appear between energy (SDG7) and alternative sustainable development goals show that, in general, positive interactions are more important than negative ones, even though these negative interactions exist [79]. To mention a few, an increased use of renewable energy sources imply also positive synergies with SDG9 (industry, innovation and infrastructure) by the financial and technical support given to the development of renewable energy sources and energy efficient infrastructure. On the other hand, in some cases, negative impacts have appeared in the past, such as the relationship between large-scale bioenergy production and agriculture or food distribution, SDG2 (Food security and agricultural productivity) as shown in the bibliography [79]. Thus, a detailed analysis of the different relations between a proposal such as the one presented in this paper and the whole set of sustainable development goals is challenging because of all the different dimensions which must be analyzed such as ocean use planning, operational risk analysis, economical analysis of the solution to name a few, including also the positive and negative impacts due to alternative energy sources [79]. This is outside the objectives of this paper and there are different frameworks which are currently developing this kind of studies [81] which could be performed in the future, when a particular installation is being designed.

5. Conclusions

A methodology for the selection of the optimal location of a far offshore hybrid wind and wave energy farms is proposed in this paper, focused on maximizing the auxiliary power supply role of the WECs. Furthermore, an assessment of the hydrogen production of different sized WECs in those selected locations is presented. As a result of the conducted analysis, the importance of a joint analysis of both, wind and waves regimes throughout a huge area like the Atlantic for the selection of the best location is stressed. Likewise, the necessity of adapting the design process of the WECs to the characteristics of the wave resource data at the location selected is demonstrated.

The MCA is shown to provide an adequate initial criteria for the selection of the location of far offshore hybrid energy farms. The first singular vector presents areas characterized by positive covariances over the whole Atlantic basin. This explains a 79% of the total covariance, so that it is to be expected that the production of hydrogen is relatively constant for the different points, as shown in Fig. 9. However, the corresponding daily temporal expansion coefficient presents a very strong seasonal behaviour (Fig. 12), which means that this is strongly predictable over the full Atlantic basin. The second mode (8% of basin-wide total covariance of daily WPD and WEF) shows a meridional dipolar structure which is related to the AO or NAO oscillations. It indicates that during positive WPD and WEF anomalies over the northern Atlantic, negative anomalies are to be expected over the southern basin. The obtained results show that locations with low covariance between WPD and WEF, particularly P-02, are the most adequate for the installation of a wind and wave hybrid energy farm. As a result of the higher variability of the wind speed in those locations, the disconnection times of the HAWTs are more prolonged and the auxiliary hydrogen generation coming from the WECs is greater and more essential. In addition, in all selected and analysed far offshore locations, the wave energy has been found to have a rather constant trend and a limited variability during the last 10 years, which proves its utility to be used as a reliable energy resource.

Finally, the characteristics of the wave resource in a given location has been found to be an important factor to be considered in the design and the selection of the geometry of the WEC to be installed. The obtained results show a direct relation between the size of the WEC and the peak periods T_p associated to the maximum power absorption of the device. Consequently, the design of the WEC should be directly related to the wave resource in that location. The installation of WECs with reduced dimensions could not only result in a lower economical cost of the device, but would also simplify its mooring and the design of the far offshore floating platform, the restraints of which are expected to be added to a more complex methodology to be developed in future works. Although the focus of this study has been the Atlantic, the MCA methodology could be applied to any other oceanic location of the world to identify an optimal location, while the conclusions regarding the appropriate dimensioning of the WEC would also remain valid for other basins with similar wave regimes.

An initial assessment of the predictability of the coupled wind and wave energy resource has been presented based on the cross-correlation functions of the expansion MCA coefficients. This opens a path for future studies in the field.

CRediT authorship contribution statement

Aitor Saenz-Aguirre: Methodology, Software, Writing - original draft, Writing - review & editing. **Jon Saenz:** Conceptualization, Methodology, Software, Writing - original draft, Writing - review & editing. **Alain Ulazia:** Conceptualization, Supervision, Writing - original draft. **Gabriel Ibarra-Berastegui:** Investigation, Supervision, Writing - review & editing.

Declaration of Competing Interest

The authors declare that they have no known competing financial interests or personal relationships that could have appeared to influence the work reported in this paper.

Acknowledgments

This paper is part of project PID2020-116153RB-I00 funded by

MCIN/AEI/ 10.13039/501100011033. Authors also acknowledge financial support by the University of the Basque Country under the contract (UPV/EHU, GIU20/008).

References

[1] Magagna D, Uihlein A. Ocean energy development in europe: Current status and future perspectives. Int J Marine Energy 2015;11:84–104.
[2] Díaz H, Soares CG. Review of the current status, technology and future trends of offshore wind farms. Ocean Eng 2020;209:107381.
[3] Babarit A, Hals J, Muliawan M, Kurniawan A, Moan T, Krokstad J. Numerical benchmarking study of a selection of wave energy converters. Renewable Energy 2012;41:44–63.
[4] R. Kempner, Ocean energy technology brief 4, International Renewable Energy Agency–IRENA.
[5] A. d. O. Falcao, Wave energy utilization: A review of the technologies, Renewable and sustainable energy reviews 14 (3) (2010) 899–918.
[6] Blanco M, Lafoz M, Ramirez D, Navarro G, Torres J, Garcia-Tabares L. Dimensioning of point absorbers for wave energy conversion by means of differential evolutionary algorithms. IEEE Trans Sustainable Energy 2018;10(3):1076–85.
[7] Cappelli L, Marignetti F, Mattiazzo G, Giorcelli E, Bracco G, Carbone S, Attaianese C. Linear tubular permanent-magnet generators for the inertial sea wave energy converter. IEEE Trans Ind Appl 2013;50(3):1817–28.
[8] Boren BC, Lomonaco P, Batten BA, Paasch RK. Design, development, and testing of a scaled vertical axis pendulum wave energy converter. IEEE Trans Sustainable Energy 2016;8(1):155–63.
[9] Piscopo V, Benassai G, Della Morte R, Scamardella A. Cost-based design and selection of point absorber devices for the mediterranean sea. Energies 2018;11(4):946.
[10] Amann KU, Magaña ME, Sawodny O. Model predictive control of a nonlinear 2-body point absorber wave energy converter with estimated state feedback. IEEE Trans Sustainable Energy 2014;6(2):336–45.
[11] Richter M, Magana ME, Sawodny O, Brekken TK. Nonlinear model predictive control of a point absorber wave energy converter. IEEE Trans Sustainable Energy 2012;4(1):118–26.
[12] Na J, Li G, Wang B, Herrmann G, Zhan S. Robust optimal control of wave energy converters based on adaptive dynamic programming. IEEE Trans Sustainable Energy 2018;10(2):961–70.
[13] de la Villa Jaén A, Santana AG, et al. Improvements in the reactive control and latching control strategies under maximum excursion constraints using short-time forecast. IEEE Trans Sustainable Energy 2015;7(1):427–35.
[14] Ashuri T, Zaaijer MB, Martins JR, Zhang J. Multidisciplinary design optimization of large wind turbines–technical, economic, and design challenges. Energy Convers Manage 2016;123:56–70.
[15] R. James, M.C. Ros, Floating offshore wind: market and technology review, The Carbon Trust 439.
[16] Babarit A, Gilloteaux J-C, Clodic G, Duchet M, Simoneau A, Platzer MF. Techno-economic feasibility of fleets of far offshore hydrogen-producing wind energy converters. Int J Hydrogen Energy 2018;43(15):7266–89. https://doi.org/10.1016/j.ijhydene.2018.02.144. URL:http://www.sciencedirect.com/science/article/pii/S0360319918306475.
[17] L. Ramírez, D. Fraile, G. Brindley, Offshore wind in europe: Key trends and statistics 2019.
[18] Babarit A, Clodic G, Delvoye S, Gilloteaux J-C. Exploitation of the far-offshore wind energy resource by fleets of energy ships – part 1: Energy ship design and performance. Wind Energy Sci 2020;5(3):839–53. https://doi.org/10.5194/wes-5-839-2020. URL:https://wes.copernicus.org/articles/5/839/2020/.
[19] Zhao C, Thies PR, Ye Q, Lars J. System integration and coupled effects of an owt/wec device. Ocean Eng 2020:108405.
[20] Astariz S, Iglesias G. Co-located wind and wave energy farms: Uniformly distributed arrays. Energy 2016;113:497–508.
[21] Gaughan E, Fitzgerald B. An assessment of the potential for co-located offshore wind and wave farms in ireland. Energy 2020;117526.
[22] Rusu E, Onea F. An assessment of the wind and wave power potential in the island environment. Energy 2019;175:830–46.
[23] Chen X, Wang K, Zhang Z, Zeng Y, Zhang Y, O'Driscoll K. An assessment of wind and wave climate as potential sources of renewable energy in the nearshore shenzhen coastal zone of the south china sea. Energy 2017;134:789–801.
[24] Ferrari F, Besio G, Cassola F, Mazzino A. Optimized wind and wave energy resource assessment and offshore exploitability in the mediterranean sea. Energy 2020;190:116447.
[25] Yee Mah AX, Ho WS, Hassim MH, Hashim H, Liew PY, Muis ZA. Targeting and scheduling of standalone renewable energy system with liquid organic hydrogen carrier as energy storage. Energy 2021;218:119475. https://doi.org/10.1016/j.energy.2020.119475. URL:http://www.sciencedirect.com/science/article/pii/S0360544220325822.
[26] Zhang W, Maleki A, Rosen MA, Liu J. Optimization with a simulated annealing algorithm of a hybrid system for renewable energy including battery and hydrogen storage. Energy 2018;163:191–207. https://doi.org/10.1016/j.energy.2018.08.112. URL:http://www.sciencedirect.com/science/article/pii/S0360544218316487.
[27] Herdem MS, Mazzeo D, Matera N, Wen JZ, Nathwani J, Hong Z. Simulation and modeling of a combined biomass gasification-solar photovoltaic hydrogen production system for methanol synthesis via carbon dioxide hydrogenation. Energy Convers Manage 2020;219:113045.
[28] Tlili O, Mansilla C, Robinius M, Syranidis K, Reuss M, Linssen J, André J, Perez Y, Stolten D. Role of electricity interconnections and impact of the geographical scale on the french potential of producing hydrogen via electricity surplus by 2035. Energy 2019;172:977–90. https://doi.org/10.1016/j.energy.2019.01.138. URL: http://www.sciencedirect.com/science/article/pii/S0360544219301549.
[29] E. Comission, A hydrogen strategy for a climate neutral europe, Press corner. URL: https://ec.europa.eu/commission/presscorner/detail/en/FS_20_1296.
[30] Temeev AA, Belokopytov VP, Temeev SA. An integrated system of the floating wave energy converter and electrolytic hydrogen producer. Renewable Energy 2006;31(2):225–39.
[31] M.F. Platzer, N. Sarigul-Klijn, J. Young, M.A. Ashraf, J.C.S. Lai, Renewable Hydrogen Production Using Sailing Ships, Journal of Energy Resources Technology 136 (2), 021203. arXiv:https://asmedigitalcollection.asme.org/energyresources/article-pdf/136/2/021203/6144716/jert_136_02_021203.pdf, doi:10.1115/1.4026200. URL:https://doi.org/10.1115/1.4026200.
[32] A. Colucci, V. Boscaino, G. Cipriani, D. Curto, V. Di Dio, V. Franzitta, M. Trapanese, A. Viola, An inertial system for the production of electricity and hydrogen from sea wave energy, in: OCEANS 2015-MTS/IEEE Washington, IEEE, 2015, pp. 1–10.
[33] Crivellari A, Cozzani V, Dincer I. Exergetic and exergoeconomic analyses of novel methanol synthesis processes driven by offshore renewable energies. Energy 2019;187:115947. https://doi.org/10.1016/j.energy.2019.115947. URL:http://www.sciencedirect.com/science/article/pii/S0360544219316317.
[34] Babarit A, Delvoye S, Clodic G, Gilloteaux J-C. Exploitation of the far-offshore wind energy resource by fleets of energy ships. part b. cost of energy. Wind Energy Sci Discussions 2020 (2020):1–13. https://doi.org/10.5194/wes-2019-101. URL: https://wes.copernicus.org/preprints/wes-2019-101/.
[35] H. Hersbach, B. Bell, P. Berrisford, S. Hirahara, A. Horányi, J. Muñoz-Sabater, J. Nicolas, C. Peubey, R. Radu, D. Schepers, A. Simmons, C. Soci, S. Abdalla, X. Abellan, G. Balsamo, P. Bechtold, G. Biavati, J. Bidlot, M. Bonavita, G. De Chiara, P. Dahlgren, D. Dee, M. Diamantakis, R. Dragani, J. Flemming, R. Forbes, M. Fuentes, A. Geer, L. Haimberger, S. Healy, R.J. Hogan, E. Hólm, M. Janisková, S. Keeley, P. Laloyaux, P. Lopez, C. Lupu, G. Radnoti, P. de Rosnay, I. Rozum, F. Vamborg, S. Villaume, J.-N. Thépaut, The era5 global reanalysis, Quarterly Journal of the Royal Meteorological Society n/a (n/a). doi:10.1002/qj.3803.
[36] M.O. Molina, C. Gutiérrez, E. Sánchez, Comparison of ERA5 surface wind speed climatologies over Europe with observations from the HadISD dataset, International Journal of Climatology 41 4864–4878. doi:10.1002/joc.7103.
[37] G.N. Petersen, Meteorological buoy measurements in the Iceland Sea 2007-2009, supplement to: Petersen, GN (2017): Meteorological buoy measurements in the Iceland Sea, 2007-2009. Earth System Science Data, 9(2), 779-789, https://doi.org/10.5194/essd-9-779-2017 (2017). doi:10.1594/PANGAEA.876206. URL: https://doi.org/10.1594/PANGAEA.876206.
[38] Contestabile P, Ferrante V, Vicinanza D. Wave energy resource along the coast of santa catarina (brazil). Energies 2015;8(12):14219–43.
[39] Alonso R, Jackson M, Santoro P, Fossati M, Solari S, Teixeira L. Wave and tidal energy resource assessment in uruguayan shelf seas. Renewable Energy 2017;114:18–31.
[40] Ribeiro A, Costoya X, de Castro M, Carvalho D, Dias JM, Rocha A, Gomez-Gesteira M. Assessment of hybrid wind-wave energy resource for the nw coast of iberian peninsula in a climate change context. Appl Sci 2020;10(21):7395.
[41] Woolf DK, Challenor PG, Cotton PD. Variability and predictability of the north atlantic wave climate. J Geophys Res: Oceans 2002;107. 9–1–9–14.
[42] Castelle B, Dodet G, Masselink G, Scott T. Increased winter-mean wave height, variability, and periodicity in the northeast atlantic over 1949–2017. Geophys Res Lett 2018;45:3586–96.
[43] Reguero B, Losada I, Méndez F. A global wave power resource and its seasonal, interannual and long-term variability. Appl Energy 2015;148:366–80. https://doi.org/10.1016/j.apenergy.2015.03.114.
[44] https://github.com/snl-waterpower/wecopttool (accessed on 3 Nov 2020).
[45] A. Babarit, G. Delhommeau, Theoretical and numerical aspects of the open source bem solver nemoh, 2015.
[46] Thompson DWJ, Wallace JM. The arctic oscillation signature in the wintertime geopotential height and temperature fields. Geophys Res Lett 1998;25(9):1297–300. https://doi.org/10.1029/98GL00950.
[47] Hurrell JW. Decadal trends in the North Atlantic Oscillation: Regional temperatures and precipitation. Science 1995;269(5224):676–9. https://doi.org/10.1126/science.269.5224.676.
[48] Barnston AG, Livezey RE. Classification, seasonality and persistence of low-frequency atmospheric circulation patterns. Mon Weather Rev 1987;115:1083–126.
[49] Wallace JM, Gutzler DS. Teleconnections in the geopotential height field during the Northern Hemisphere winter. Mon Wea Rev 1981;109:784–812.
[50] Bretherton CS, Smith C, Wallace JM. An Intercomparison of Methods for Finding Coupled Patterns in Climate Data. J Clim 1992;5:541–60. https://doi.org/10.1175/1520-0442(1992)005<0541:AIOMFF>2.0.CO;2.
[51] C.K. Parise, L. Farina, Ocean wave modes in the South Atlantic by a short-scale simulation, Tellus A: Dynamic Meteorology and Oceanography 64 (1) (2012) 17362. arXiv:https://doi.org/10.3402/tellusa.v64i0.17362, doi:10.3402/tellusa.v64i0.17362. URL:https://doi.org/10.3402/tellusa.v64i0.17362.
[52] Fei Z, Juan D, Jiang Z. A reconstructed wind stress dataset for climate research over the Tropical Pacific during a 153-year period. Atmospheric Oceanic Sci Lett 2009;2:277–83. https://doi.org/10.1080/16742834.2009.11446812.
[53] Dewitte B, Illig S, Renault L, Goubanova K, Takahashi K, Gushchina D, Mosquera K, Purca S. Modes of covariability between sea surface temperature and wind stress

intraseasonal anomalies along the coast of Peru from satellite observations (2000–2008). J Geophys Res: Oceans 2011;116:C04028. https://doi.org/10.1029/2010JC006495.
[54] North G, Bell T, Cahalan R, Moeng F. Sampling errors in the estimation of empirical orthogonal functions. Mon Weather Rev 1982;110:699–706. https://doi.org/10.1175/1520-0493(1982)110<0699:SEITEO>2.0.CO;2.
[55] Efron B, Tibshirani R. Bootstrap methods for standard errors, confidence intervals and other measures of statistical accuracy. Stat Sci 1986;1:54–77. http://www.jstor.org/stable/2245500.
[56] Pérez-Collazo C, Greaves D, Iglesias G. A review of combined wave and offshore wind energy. Renew Sustain Energy Rev 2015;42:141–53.
[57] Karimirad M. Offshore energy structures: for wind power, wave energy and hybrid marine platforms. Springer; 2014.
[58] Chen W, Gao F, Meng X, Chen B, Ren A. W2p: A high-power integrated generation unit for offshore wind power and ocean wave energy. Ocean Eng 2016;128:41–7.
[59] Tsujimoto M, Uehiro T, Esaki H, Kinoshita T, Takagi K, Tanaka S, Yamaguchi H, Okamura H, Satou M, Minami Y. Optimum routing of a sailing wind farm. J Marine Sci Technol 2009;14(1):89–103.
[60] D. Snyder, B. Townsley, Ss: Perdido development project: World, in: Offshore Technology Conference, OnePetro, 2010.
[61] Faizal M, Ahmed MR, Lee Y-H. A design outline for floating point absorber wave energy converters. Adv Mech Eng 2014;6:846097.
[62] Coe RG, Bacelli G, Olson S, Neary VS, Topper MB. Initial conceptual demonstration of control co-design for wec optimization. J Ocean Eng Marine Energy 2020:1–9.
[63] J. Jonkman, S. Butterfield, W. Musial, G. Scott, Definition of a 5-mw reference wind turbine for offshore system development, Tech. rep., National Renewable Energy Lab.(NREL), Golden, CO (United States) (2009).
[64] Rusu E, Onea F. A review of the technologies for wave energy extraction. Clean Energy 2018;2(1):10–9.
[65] Saenz-Aguirre A, Ulazia A, Ibarra-Berastegui G, Saenz J. Extension and improvement of synchronous linear generator based point absorber operation in high wave excitation scenarios. Ocean Eng 2021;239:109844.
[66] Iles C, Hegerl G. Role of the North Atlantic Oscillation in decadal temperature trends. Environ Res Lett 2017;12:114010. https://doi.org/10.1088/1748-9326/aa9152.
[67] Ulazia A, Penalba M, Rabanal A, Ibarra-Berastegi G, Ringwood J, Sáenz J. Historical evolution of the wave resource and energy production off the chilean coast over the 20th century. Energies 2018;11(9):2289.
[68] Mentaschi L, Vousdoukas MI, Voukouvalas E, Dosio A, Feyen L. Global changes of extreme coastal wave energy fluxes triggered by intensified teleconnection patterns. Geophys Res Lett 2017;44:2416–26. https://doi.org/10.1002/2016GL072488.
[69] Cortesi M, Torralba V, González-Reviriego N, Soret A, Doblas-Reyes FJ. Characterization of European wind speed variability using weather regimes. Clim Dyn 2019;53:4961–76. https://doi.org/10.1007/s00382-019-04839-5.
[70] François B. Influence of winter North-Atlantic Oscillation on climate-related-energy penetration in Europe. Renewable Energy 2016;99:602–13. https://doi.org/10.1016/j.renene.2016.07.010.
[71] Saenz J, Rodriguez-Puebla C, Fernandez J, Zubillaga J. Interpretation of interannual winter temperature variations over southwestern Europe. J Geophys Res: Atmospheres 2001;106(D18):20641–51. https://doi.org/10.1029/2001JD900247.
[72] Ulazia A, Sáenz J, Ibarra-Berastegi G, González-Rojí SJ, Carreno-Madinabeitia S. Global estimations of wind energy potential considering seasonal air density changes. Energy 2019;187:115938. https://doi.org/10.1016/j.energy.2019.115938.
[73] Sippel S, Meinshausen N, Fischer EM, Székely E, Knutti R. Climate change now detectable from any single day of weather at global scale. Nat Clim Chang 2020;10:35–41. https://doi.org/10.1038/s41558-019-0666-7.
[74] Dresp S, Dionigi F, Klingenhof M, Strasser P. Direct electrolytic splitting of seawater: opportunities and challenges. ACS Energy Letters 2019;4(4):933–42.
[75] F. Timmermans, https://www.fch.europa.eu/news/european-green-deal-hydrogen-priority-area-clean-and-circular-economy, (accessed on 13 Jan 2021).
[76] General Assembly of the United Nations, 70/1. Transforming our world: the 2030 Agenda for Sustainable Development, A/RES/70/1 (2015).
[77] Keivanpour S, Ramudhin A, Kadi DA. The sustainable worldwide offshore wind energy potential: A systematic review. J Renewable Sustainable Energy 2017;9:065902. https://doi.org/10.1063/1.5009948.
[78] Falcone PM, Hiete M, Sapio A. Hydrogen economy and sustainable development goals: Review and policy insights. Current opinion Green Sustainable Chem 2021;31:100506. https://doi.org/10.1016/j.cogsc.2021.100506.
[79] McCollum DL, Gómez-Echeverri L, Busch S, Pachauli S, Parkinson S, Rogelj J, Krey V, Minx JC, Nilsson M, Stevance A-S, Riahi K. Connecting the sustainable development goals by their energy inter-linkages. Environ Res Lett 2018;13:033006. https://doi.org/10.1088/1748-9326/aaafe3.
[80] Lee K-H, Noh J, Khim JS. The Blue Economy and the United Nations' sustainable development goals: Challenges and opportunties. Environ Int 2020;137:105528. https://doi.org/10.1016/j.envint.2020.105528.
[81] J. castor, K. Bacha, F.F. Nerini, Sdgs in action: A novel framework for assessing energy projects against the sustainable development goals, Energy Research & Social Science 68 (2020) 101556. doi:10.1016/j.erss.2020.101556.